Mar Geophys Res (2006) 27:267–281
DOI 10.1007/s11001-006-9007-0

ORIGINAL PAPER

First results from the North Iceland experiment

C. Riedel · A. Tryggvason · B. Brandsdottír · T. Dahm · R. Stéfansson · M. Hensch · R. Böðvarsson · K. S. Vogfjord · S. Jakobsdottír · T. Eken · R. Herber · J. Holmjarn · M. Schnese · M. Thölen · B. Hofmann · B. Sigurdsson · S. Winter

Received: 25 April 2005 / Accepted: 7 August 2006 / Published online: 14 September 2006

Abstract Between June 2004 and September 2004 a temporary seismic network was installed on the northern insular shelf of Iceland and onshore in north Iceland. The seismic setup aimed at resolving the subsurface structure and, thus, the geodynamical transition from Icelandic crust to typical oceanic crust along Kolbeinsey Ridge. The experiment recorded about 1,000 earthquakes. The region encloses the Tjörnes Fracture Zone containing the Husavik–Flatey strike-slip fault and the extensional seismic Grimsey Lineament. Most of the seismicity occurs in swarms offshore. Preliminary results reveal typical mid-ocean crust north of Grimsey and a heterogeneous structure with major velocity anomalies along the seismic lineaments and north–south trending subsurface features. Complementary bathymetric mapping highlight numerous extrusion features along the Grimsey Lineament and Kolbeinsey Ridge. The seismic dataset promises to deliver new insights into the tectonic framework for earthquakes in an extensional transform zone along the global mid-ocean ridge system.

Keywords Broadband seismology · Multibeam bathymetry · Hot spot-ridge interaction · Iceland · Ocean bottom seismology · Tjörnes fracture zone

C. Riedel · T. Dahm · M. Hensch · R. Herber · M. Schnese · M. Thölen · B. Hofmann · S. Winter
Institut für Geophysik, Bundesstr. 55, 20146 Hamburg, Germany

A. Tryggvason · R. Böðvarsson · T. Eken
Institutionen för Geovetenskaper, Avdelningen för Geofysik, Villavägen 16, 75236 Uppsala, Sweden

B. Brandsdottír
Science Institute, University of Iceland, Öskju, Sturlugata 7, 101 Reykjavík, Iceland

R. Stéfansson · K. S. Vogfjord · S. Jakobsdottír · J. Holmjarn
Physics Department, Meteorological Office of Iceland, Bustadavegur 9, 150 Reykjavík, Iceland

B. Sigurdsson
Marine Research Institute, Skulagata 4, 121 Reykjavík, Iceland

Present Address:
C. Riedel (✉)
Centro de Vulcanologia e Avaliaçao dos Riscos Geologicos, Ponta Delgada, Açores, Portugal
e-mail: carsten.riedel@azores.gov.pt

Introduction

The north of Iceland represents in many ways an extraordinary geological setting. In 1974, Sæmundsson gave a first good tectonic and geological description of a region where the Mid-Oceanic Ridge changes from an offshore to an onshore ridge, separated by a transform zone. However, this transform zone is leaky and shortly after publishing the geological review of Sæmundsson (1974) a subaerial fissure eruption along the Krafla fissure swarm (Fig. 1) between 1973 and 1983 revealed its volcanic potential. Strong earthquakes above magnitude 7 make it the primary focus of high-energetic seismicity in and around Iceland. Whereas this produced high attention in the scientific community its offshore situation in contrast to the onland transition in the south Iceland Seismic Zone requires considerably more effort to reveal its detailed tectonic setup. With our study we try to contribute to this effort.

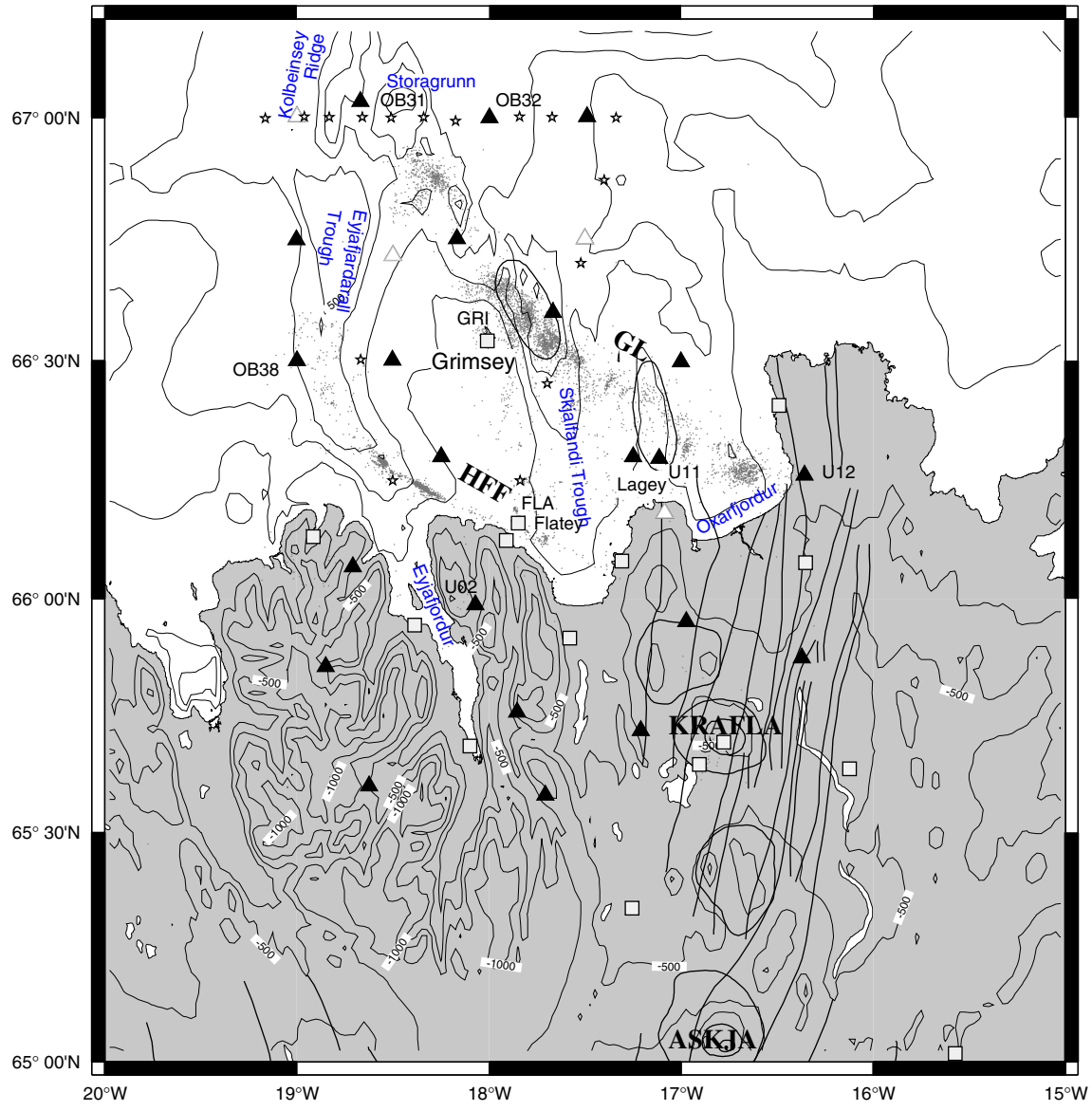

Fig. 1 Map of bathymetry and topography of North Iceland, indicating the main historicalvolcanic centers Krafla and Askja, the permanent stations of the Icelandic network (*grey squares*) and the temporary stations (*black triangles*) of our experiment, the shot locations (*stars*) and the two well-known seismic lineaments Husavik–Flatey fault (*HFF*) and Grimsey lineament (*GL*). Some seismic stations, islands and morphologic deeps have been marked because they are further discussed in the text. To allow for further notation, the depth contours offshore start at 200 m depth and are sampled in 100 m. The altitude contours on land are sampled in 250 m

Whereas the Krafla system is still considered part of the North Volcanic Zone (NVZ) of Iceland (Björnsson et al. 1977), which trends into Öxarfjörður bay, some kilometers offshore in the western part of this bay two islands—the Mánareyjar islands Lagey (Fig. 1) and Háey—tower above a north–south trending bathymetric ridge extending up to 66°30 N. This ridge probably featured a volcanic eruption at the end of the 19th century (1867/1868; see Thoroddsen 1925). The bathymetry is dominated by north–south trending troughs and ridges, which following the crest of the ridges from the south to the north are always offset to the west before finally joining with the central rift of Kolbeinsey Ridge at around 67°N (see Fig. 1). Kolbeinsey Ridge shares most characteristics of the typical Mid-Atlantic Ridge sections and arctic ridges. It is slow-spreading (Vogt et al. 1980) and produces tholeiitic rocks with MgO content of 6–10 wt.% (Devey et al. 1994), which is often termed a depleted, but still normal mid-ocean ridge basalt (N-MORB).

The alternating bathymetry north of the Icelandic coast is a morphological result of en echelon normal faulting (Sæmundsson 1974; McMaster et al. 1977; Rögnvaldsson et al. 1998) following shearing between the spreading regimes of Kolbeinsey Ridge and the NVZ (Gudmundsson et al. 1993). Within the pull-apart basins, one of them forming a major bathymetric low-located just east of Grimsey (see Fig. 1), gaseous pockmarks are observed (Richter et al. 2003). Their number increases toward the major permeable faults as, e.g. the Husavik–Flatey fault (HFF on Fig. 1). Fluid migration along the faults also feeds high-temperature hydrothermal fields (e.g. Botz et al. 1999; Riedel et al. 2001), which built hydrothermal smokers of more than 60 m height in Eyjafjordur (Stoffers et al. 1997). Small volcanic cones of around 300 m base diameter and smaller (Kuhn et al. revised) have been imaged along the Grimsey Lineament (GL on Fig. 1), a seismic lineament parallel to and north of the HFF. A major submarine volcanic structure of around 8 km base diameter is Storagrunn (Fig. 1) just north of 67°N. This structure has a characteristic shield volcano slope of 2° on average mapped by multibeam bathymetry surveys by Brandsdottir et al. (2002, 2004).

Between Askja volcano and Grimsey island the transform zone is monitored by the permanent seismic South Iceland Lowland (SIL) network (grey squares on Fig. 1: Rögnvaldsson et al. 1998) and permanent GPS stations (Geirsson 2002) from the Meteorological Office of Iceland. The crustal structure has been analyzed by local earthquake tomography (LET) of the SIL seismic travel-time data (Riedel et al. revised). The results reveal a negative velocity anomaly reaching down to 12 km depth along the main rupture of the transform zone, the HFF. A further negative anomaly between Flatey (Fig. 1) and Grimsey, covering a depth to 12 km has been suggested to mirror an alignment of magma bodies or a high heat-flow domain. However, in the submarine parts the shallow subsurface cannot be resolved by the permanent seismic network, and therefore most parts of the GL is not imaged above 8 km.

A main point of discussion is the precise position of the plate boundary. Gudmundsson et al. (1993) proposed a model of two mode I cracks (i.e. extensional zones) mirroring the two spreading domains of Kolbeinsey Ridge and NVZ. In their model the North American plate and Eurasian plate are separated along the HFF close to the northern coastline of Iceland. Taylor et al. (1994) proposed a structural boundary along the GL, which they call an extensional transform zone, i.e. along the complete boundary of North American plate and Eurasian plate spreading occurs in contrast to the Gudmundsson et al. (1993), where real strike-slip transform motion occurs. Taylor et al. (1994) compared oblique spreading regimes and extensional transform zones worldwide and concluded that the HFF is acting as a secondary fault, i.e. a Riedel shear, with respect to the North America–Eurasia transforms in a similar fashion as the San Andreas fault joins with the Mendocino Fracture Zone in the Pacific (Hole et al. 2000).

The purpose of this study is to analyze the transition from Iceland to Kolbeinsey Ridge by a coupled seismic and multibeam bathymetry survey. The seismic experiment was aimed to improve hypocenter locations and LET results by using ocean bottom seismometers (OBS) and a temporal extension of the station setup on land. The bathymetric data close some of the gaps in the multibeam bathymetric map of the Tjörnes Fracture Zone and provide a unique view on the bathymetry of the southern end of Kolbeinsey Ridge.

Survey

In a joint effort by Hamburg University, Uppsala University and the Icelandic Meteorological Office between June 25 and July 8, 2004, the permanent seismic network was expanded by 25 additional stations (see black triangles on Fig. 1). Of these 14 were seismic ocean-bottom stations (OB30–OB43 see Tables 1, 2) and 11 seismic land stations (U2–U12 see

Table 1 Positions of the temporary seismic network stations

Station	Latitude	Longitude	Depth (–)/ Elevation (+) in m
OB31	67°01.942N	18°40.193W	–312
OB32	66°59.988N	17°59.998W	–438
OB33	67°00.006N	17°29.390W	–274
OB34	66°44.975N	19°00.007W	–489
OB36	66°45.160N	18°10.300W	–370
OB38	66°29.942N	18°59.877W	–485
OB39	66°30.079N	18°30.269W	–157
OB40	66°35.999N	17°40.160W	–242
OB41	66°29.911N	17°00.063W	–238
OB42	66°17.960N	18°14.770W	–107
OB43	66°18.000N	17°15.008W	–154
U2	65°59.238N	18°04.320W	273
U3	65°51.360N	18°51.090W	275
U4	65°45.558N	17°51.318W	289
U5	65°57.144N	16°58.416W	290
U6	65°36.060N	18°37.512W	309
U7	65°43.140N	17°12.600W	159
U8	66°04.098N	18°42.558W	162
U9	65°52.494N	16°22.326W	321
U10	65°34.854N	17°42.366W	315
U11	66°15.636N	16°21.480W	67
U12	66°17.790N	17°06.942W	22

Table 2 The sensors used and their sample rates

Stations	Datalogger	Sensor	Sample rate
OB30–OB33	SEND Geolon MLS	OAS Hydrophone (one component: h)	50 Hz
OB34–OB43	GeoPro SEDIS III	Hydrophone/Seismometer (four components: Z, N, E and h)	128 Hz
U2	EarthData logger	Lennartz LE-1s (three components: Z, N and E)	100 Hz
U3–U12	EarthData logger	Lennartz LE-5s (three components: Z, N and E)	100 Hz

Tables 1, 2). The ten short-period OBS from GeoPro and four broadband ocean bottom hydrophones (OBH) from the University of Hamburg were deployed from R/V Drofn during its final cruise. The 11 seismic land stations from the University of Uppsala were positioned between 19°W and 16°W and north of 65°30′N. One of them was installed on Lágey Island (see Fig. 1).

With the exception of U12 (Fig. 1) all stations were up and running during an active source experiment that was carried out using 16 shots of 22.8–45.6 kg dynamite in the water column (see white stars on Fig. 1). Compressors for large volume airguns are not easily available on the sparsely populated North Atlantic Island.

Technical details and positions for the seismic stations are given in Tables 1 and 2. During the cruise R/V Arni Fridriksson A 13, 2004 between September 6 and September 17, 2004, the OBS and OBH were recovered from the seabed. Three stations (OB30, OB35 and OB37, marked as white triangles on Fig. 1) failed to deliver data, one because of a datalogger drifting into saturation and the other two because water penetrated the glass spheres, which covered the seismometers. Due to power failure of the EarthData logger, the station U11 on Lágey only recorded 6 weeks of data. However, including the permanent SIL network, recordings from up to 36 stations are available for some of the bneraly 1,000 recorded events during the period of operation.

After recovery of the seismic stations, the multibeam sounding equipment of R/V Arni Fridriksson was used to expand the extensive multibeam survey of the Tjörnes Fracture Zone started by Brandsdottir and others in earlier cruises (Brandsdottir et al. 2002; Richter et al. 2003). Particularly the region north of 67 N, in Eyjafjordur and surrounding Storagrunn volcano was covered. A fine-scale morphology down to a lateral resolution of some meters on top of Storagrunn volcano was obtained. Analysis of multibeam bathymetry data is particularly dependent on the acoustic velocity profile in the water column. Therefore 11 conductivity–temperature–depth (CTD) profiles were acquired during the survey (see Table 3) down to a maximum depth of about 450 m.

Table 3 Map of CTD positions and deployment times and dates

CTD No	Latitude N	Longitude W	Deployment time
298	66°13.07	17°40.85	21:46:01, 06/09/04
299	66°45.17	17°30.08	19:48:38, 07/09/04
300	67°01.17	17°55.65	23:22:47, 07/09/04
301	66°53.67	19°14.53	20:59:50, 08/09/04
302	67°30.24	18°59.67	02:19:41, 09/09/04
303	67°30.08	18°41.82	23:07:27, 09/09/04
304	67°01.90	18°24.82	21:20:47, 10/09/04
307	66°15.84	16°51.46	14:13:50, 11/09/04
308	65°49.35	18°07.76	21:17:12, 12/09/04
309	65°53.93	18°13.64	23:05:06, 12/09/04
310	66°07.68	18°29.50	01:12:35, 13/09/04

The top and flanks of Storagrunn were dredged, but during dredging of the suggested recent lava flows east of the volcano, unfortunately the dredge was lost. The rocks recovered were all allochthonous material, probably beach gravel or glacially transported boulders.

Data processing

Seismic data

The seismic data set is heterogeneous (Fig. 2). Data was sampled at different sample rates on different kinds of instruments (Table 2) and stored in different formats ranging from miniSeed to internal formats. The land stations (EarthData loggers) were synchronized every half hour with the Global Positioning system (GPS). GPS reception was unproblematic on northern Iceland and implied that time drifts during recording were negligible. The ocean bottom registration, however, need an additional step of preprocessing. They are only communicating twice to a reference time signal, in our case the GPS time, once when deployed and once when recovered. In between, a drift of the internal clock occurs. The seismic time series data were resampled to account for this drift.

A fundamental difference in the corrections is evident for the SEND and Sedis III dataloggers (see Table 2). SEND dataloggers sample a time sequence of

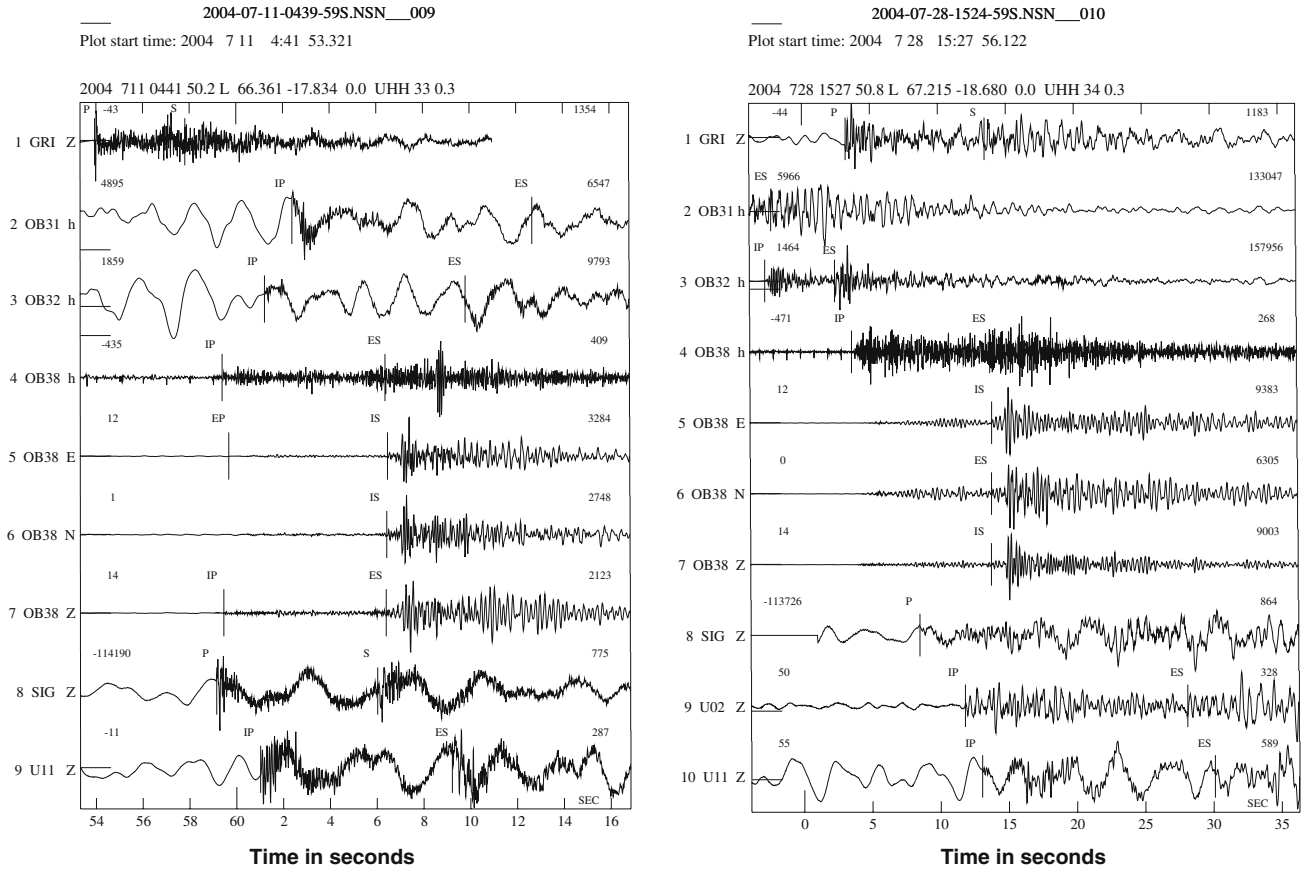

Fig. 2 Diagrams show the recordings of the seismic network on a day with rough weather and sea conditions (left) and on a quieter weather day (right). The stations have been marked in Fig. 1, names are printed on the *left side* followed by component where *Z* vertical component, *N* and *E* are horizontal component and *h* refers to a hydrophone

an additional internal quartz clock with a much faster sample rate than the original data to account for the non-linear internal clock drift. In this way the overall drift can be associated with the non-linear drift, whereas the Sedis III datalogger time was corrected only by compressing the time axis linearly between deployment and recovery datum using a floating point sample rate. The maximum clock drift registered was in the order of 1.7 s over the whole duration of the experiment, which corresponds to 28 ms/day (i.e. approximately four samples).

After clock drift removal, all data including the waveforms of the detected events by the stationary SIL network were converted to GSE format and a database was constructed in SEISAN (Havskov and Ottemoller 2003). Phase readings from the automatic picking of SIL were also converted to SEISAN S-files and the associated waveforms were extracted in a narrow time window ranging from just before the suggested origin time to 2 min beyond the suggested last S pick in the record. Finally, the data were manually repicked on all stations, the permanent and the temporary ones, using the SEISAN system. This study uses SIL arrival times for the ~1,000 events recorded during the time period. These were manually corrected and extended to picks on the temporary network for all the data, which were recorded.

The seismic data acquired during the dynamite explosions (Fig. 6) was preprocessed in the same manner. The time series were rearranged to start at the GPS time recorded during the explosion and uniformly resampled to 100 Hz. These resampled time series were converted to SEG Y format and analyzed using Seismic Unix (Cohen and Stockwell 2003). For picking of the first arrival, a Hilbert transform was used on the data as, e.g. Earle and Shearer (1994), and the Butterworth bandpass filtered amplitude component (2–4–20–30 Hz) served as the pick dataset. Here, the real seismic traces are shown.

The land station positions were taken from the GPS logs of the instruments. The position was logged twice a day, and the mean positions were used. In general,

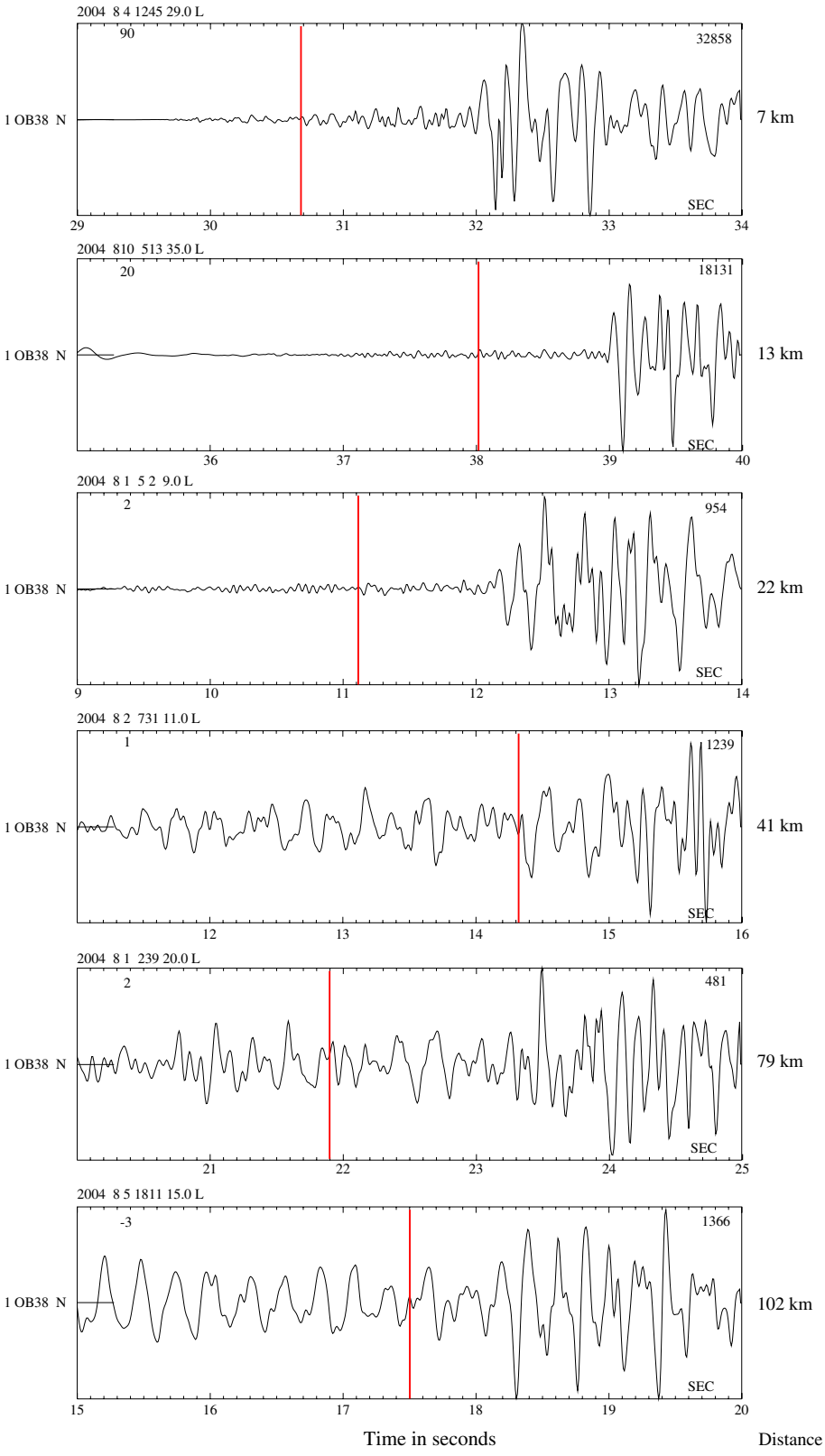

Fig. 3 The raw data from the North component of OB38 is displayed in this graph, the S pick has been marked. The maximum of the S-wave usually arrives later than the pick, due to a multiple of reasons stated in the text. The delay of the maximum of the S-wave to the pick varies with distance. All time windows displayed are 5 s long

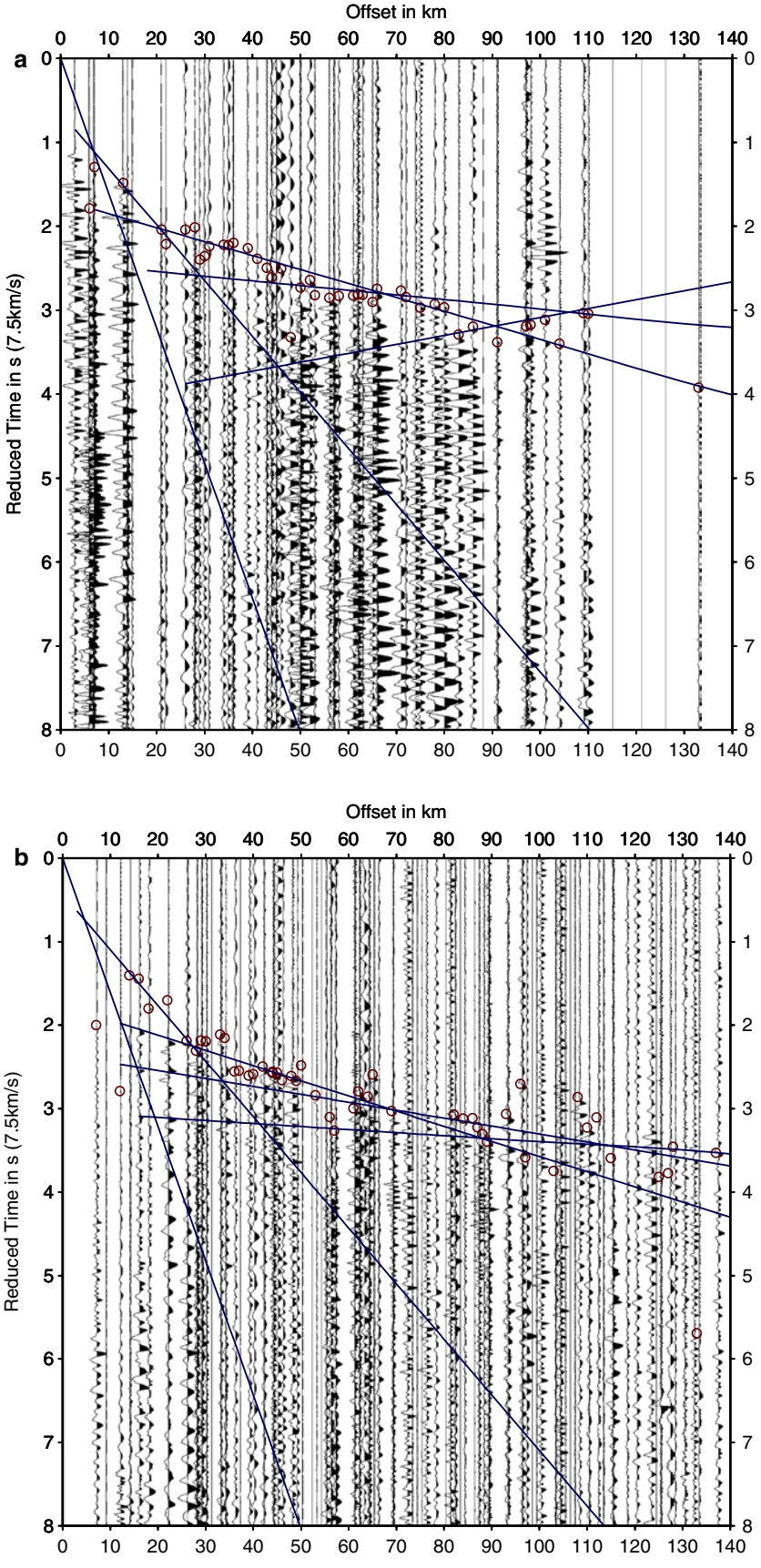

Fig. 4 Reduced time-offset sections of all recordings and shots a north of the Grimsey Lineament and b south of the Grimsey Lineament both filtered at 4–20 Hz. *Circles* mark the picked onset of the first arrival. *Lines* marks the theoretical model fitted to the section

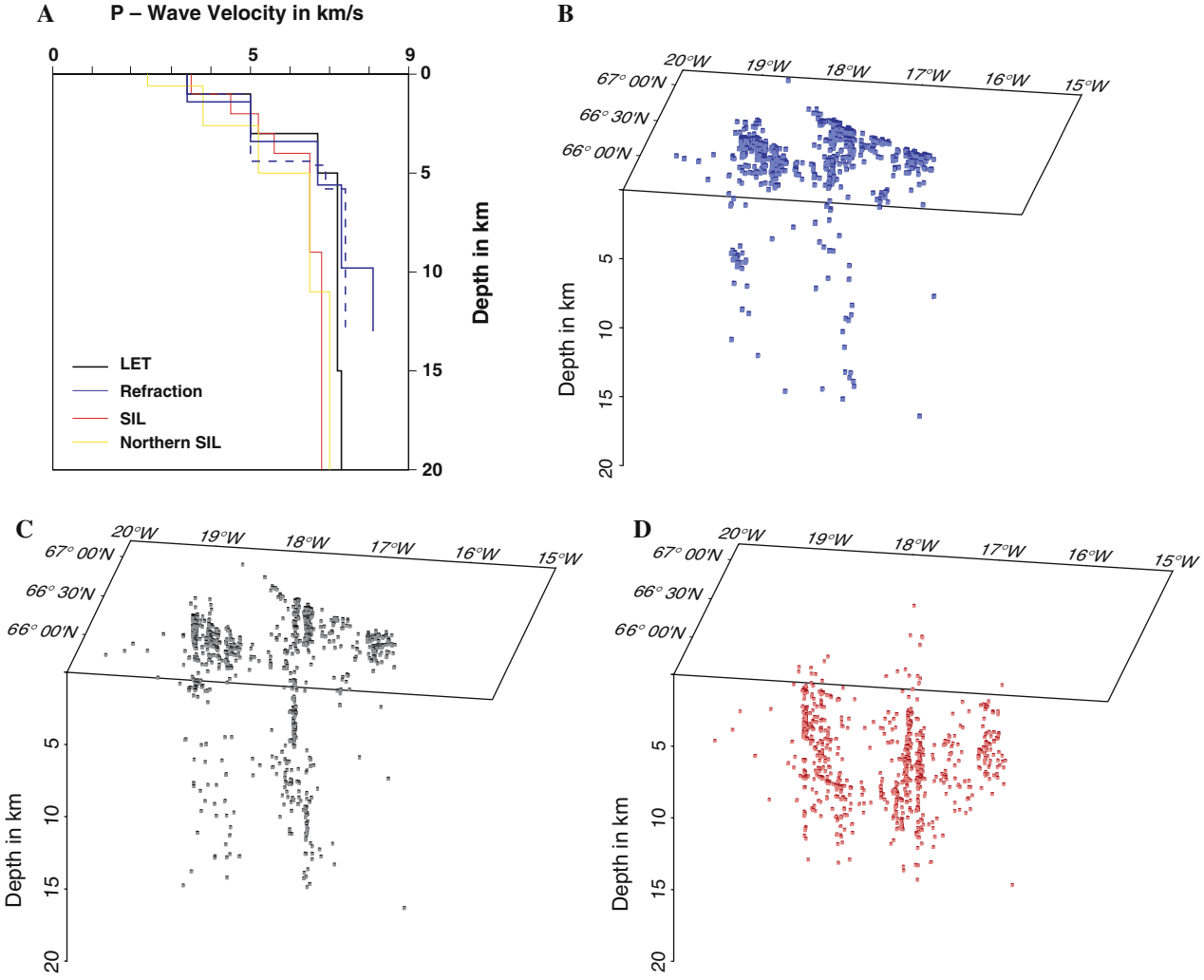

Fig. 5 (**A**) Diagram shows the compressional wave velocity models used in this study. The *solid blue* line is the refraction result north of the Grimsey Lineament (*GL*), the *dashed line* south of this lineament. The same *colors* have been used for the following plots (**B–D**), which display the location of hypocenters using the according velocity model in 3D ((**B**) refraction model north of GL, (**C**) LET model, and (**D**) SIL model). Further details see main text

the horizontal standard deviation was of the order of 3 m, and generally below 4 m vertically. The vertical positions were also compared to a digital elevation model with a resolution of 50 m (assuming the horizontal positions were correct). They agreed to within –4 m + –25 m (1σ). The OBS and OBH positions were determined as the mean position between deployment and recovery locations. The largest differences are about 0.1 min in latitude and 0.2 min in longitude, i.e. about 50–100 m. In an attempt to improve the location of OBSes from the order of 100 m to the order of 10 m, in addition to the first arrivals, we tried to pick the arrival of the water wave on the OBS recordings. This would be equivalent to a small number of samples on the time series, but would provide a result independent of the subsurface seismic velocity model. Although the water wave phases include the highest amplitudes in the seismogram, it is often hard to determine the exact onset on close inspection, so we restricted our processing to the analysis above.

Multibeam data

The multibeam data were acquired using the MB system software suite (Caress and Chayes 1995) on a UNIX machine connected to a SIMRAD EM 300 instrument aboard R/V Arni Fridriksson. From time-to-time, the sound velocity profile used for the inversion of water depth was adapted to the closest spot

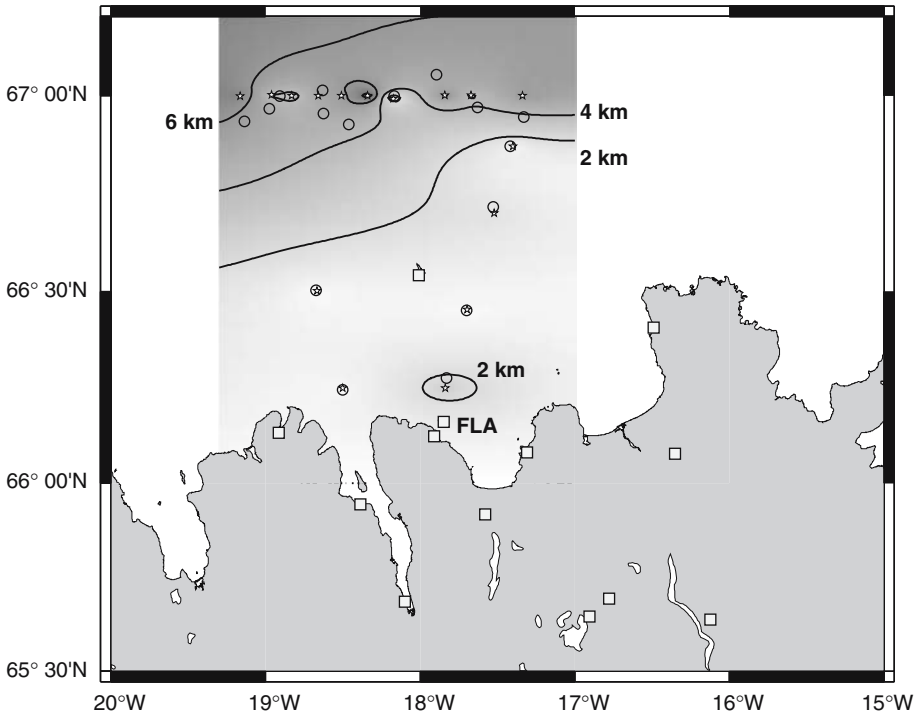

Fig. 6 Isoline and grayscale plot of the quality of locating by the permanent network. *Darker colors* refer to bigger errors. The lateral error has been used to number the *lines*, *small circles* mark the location of a shot by the network, *stars* mark the real position of the shot. The permanent stations are marked by *gray squares*

where CTD measurements were performed. These CTDs were acquired using Seabird SBEII plus equipment with an installed thermosalinograph SBE 16. Further processing is still needed and a complete bathymetric map will be published elsewhere (Brandsdottir et al. 2002, 2004). The preliminary results presented here were smoothed and interpolated by E. Kjartansson (personal communication) at the University of Iceland. An excerpt around Storagrunn volcano is shown in Fig. 7.

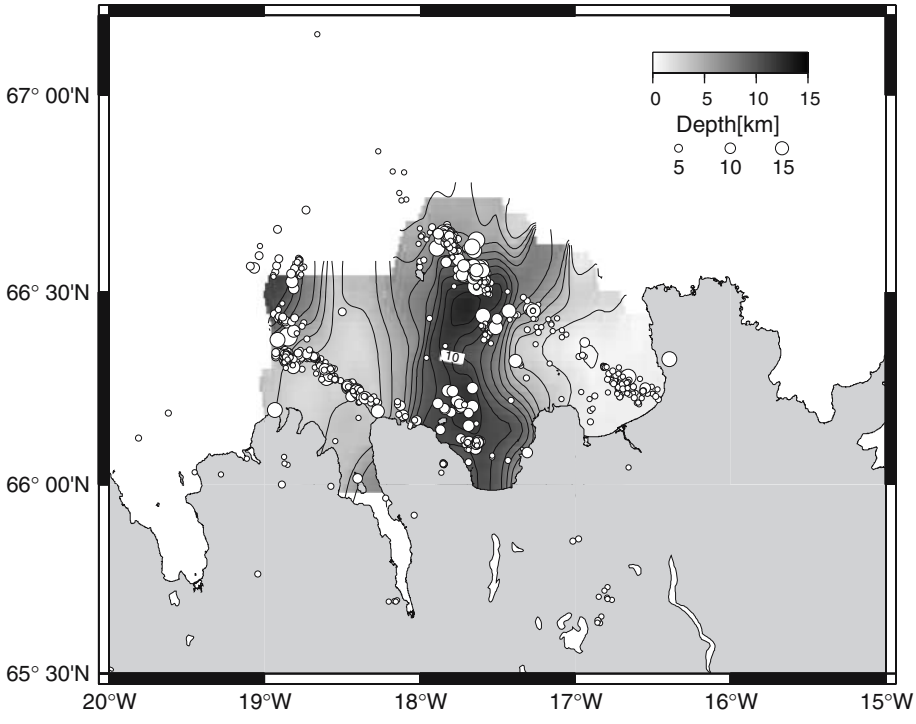

Fig. 7 *Isoline* and *grayscale* plot of the apparent maximum depth of hypocenters. This apparent maximum depth refers to the depth above which 80% of all events are located. Each event is displayed by a *small circle*. The radius of this circle is indicative of its depth. The maximum depth of events is found between Grimsey and Flatey Islands

First results

Waveforms and picks

The acquired seismic waveforms are very similar among the broadband instruments. They are subject to weather and sea conditions. On rough days (see Fig. 2a) a strong amplitude low-frequency component (about 0.5 Hz) is visible (here on stations OB31, OB32, SIG and U11 and less strong on GRI), on quiet days (see Fig. 2b) seismic signals from the subsurface dominate the time series (here on stations SIG and U11 a small amplitude low-frequency component in the overall signal is still visible due to some environmental effect). The short-period instruments (as an example OB38 in Fig. 2) are like high-pass filters implying that no microseismic noise is evident. For 10% of the events their dynamic range is very low, which is either a consequence of the noise or an electronic problem of the data logger.

Most P- and S-phases have an impulsive onset, however the first arrival is not necessarily the same on all components for the OBS data: a phenomenon that was already recognized during the TYSEA experiment (Dahm et al. 2002). This is a consequence of a ringing effect produced by the low-S velocities in the shallow underground just beneath the OBS (Thorwart and Dahm 2003). More P-phases could be picked than S-phases, but some S-phases are more impulsive than the first arrival. In rare cases, only after Butterworth bandpass filtering between 4 and 20 Hz (see above) the signal was clear enough to provide a sufficient quality picking (see Fig. 2). This is also indicated by cross-correlations of the waveforms at one station of various events within one swarm, which show a maximum when a bandpass between 4 and 20 Hz is used.

The strongest amplitude arrival for the events is not necessarily the S-wave onset (cf. OB38 on Fig. 2a). There can be an amplitude response one order higher than the S-wave onset, particularly on the hydrophone. There are several origins for this high-amplitude arrival. For large-offset arrivals the SmS and Sn phase interfere with the S-wave. For smaller offsets and short time-delays an interference effect in the shallow subsurface near the seismometer may cause a delay effect. Here, the effect is often strongest on the hydrophone, thus it might be a wave converted into an acoustic wave at the seabed, i.e. a tertiary or T-wave. Thorwart and Dahm (2003) noticed that the horizontal and vertically polarized S-waves might arrive at different times and produce a similar effect (shallow shear-wave splitting). An example is given for the North component of OB38 on Fig. 3, where the time delay changes from 1.4 s at distances of 7 km to around 0.7 s between 40 and 80 km and back to 1.4 s at distances around 100 km. This is a clear evidence that we do not simply see an S-to-P conversion, but various effects interfere.

Visual inspection suggests that the picking error for the P-wave onset on quiet days is in the order of 1–5 ms, on rough days it increases to 5–10 ms. The picking error for the S-wave is generally on the order of 5–20 ms, once the actual onset phase can be established. The time difference between onset and maximum amplitude may be in the order of seconds (cf. U02 on Fig. 2b). This time-lag effect is typical for the permanent stations GRI and FLA, where automatic picking of the S-wave is often not in accordance with the subsurface model even after correction of the S-phase pick (see, e.g. GRI on Fig. 2b, where the amplitude increases before the automatic S-pick).

Refraction seismics

The number and distribution of shots and stations is not sufficient to evaluate the subsurface structure below a single station or a single shot. Not only after the analysis of P- and S-picks of the natural seismicity do we realize that the region in study is very heterogeneous and bound to produce all sorts of seismic phenomena. However, we can reconstruct a mean 1D velocity model by averaging over two seismic sections including all shots on all stations:

- one north of the GL;
- and the other south of the GL.

Because all shots were fired north of the HFF, the different structure north and south of this structure cannot be compared in a similar way by our survey results. This trivial approach provides us with seimograms of a median spatial sampling around 1 km (Fig. 4). The first arrivals were picked (circles in Fig. 6) and by assuming a simple 1D model, the refracted arrivals using a ray-approach for homogeneous layers were fit to the data.

In the reduced time section for the region north of the GL (Fig. 4a) it is apparent that the resolution in the 20 km closest to the shot is insufficient. A linear trend in the range of 3.2–3.5 km/s seems to receive the dominant wave energy, mainly visible in later arrivals between 4 and 5 s. Latest from 10 km on, travel time picks indicate a velocity of 5 km/s. Between 20 and 65 km offset, a phase with the velocity of 6.7 km/s is apparent. Beyond 50 km the best visible trend emerges with a velocity of 7.2 km/s. Some picks in a distance range from 80 to 120 km contrain a Moho velocity of

8.15 km/s. This is the not a unique way to interpret the data, but this refraction model (blue solid line in Fig. 5) fits well to other models in the region in study (e.g. the LET model or the Kolbeinsey Ridge model of Hooft et al. 2006). The location of the Moho and the seismic velocity below the Moho remains disputable. We have simply shown it here, because we want to highlight that it is not impossible to detect a Moho north of the GL. Many late arrivals in distance ranges between 40 and 80 km align with the picks on this refractor. To cut a long story short there is no evidence for a transition layer but rather a real Moho in north of Iceland.

South of the GL (Fig. 4b) the resolution seems to be better in the first 20 km, but we are still unable to find a direct wave and selected the same velocity as the 1D LET of Riedel et al. (2005). In very decent offsets of 10 km and less, the refracted wave from a 5 km/s horizon takes over the first break character and from a distance of 30 km on the character of the picked first breaks is pretty chaotic. Some of the late arrivals help to fit a trend of 6.6, 7 and 7.3 km/s. The last phase is only apparent as the first arrival after 120 km, so we are dealing with a very slow crust in this case. This model is shown as dashed blue line in Fig. 5. It would be possible to align some phases between 110 and 140 km at a refractor velocity of 8.7 km/s, however, it seems unreasonable that a refractor with such a high velocity should appear and that it should receive so much energy, when all the other phases clearly loose energy beyond distances of 100 km. The restrictions imposed by our small dataset prevent a more thorough analysis of this phase. In any case such a high velocity implies a dip of the refractor should it exist.

Travel times, root-mean-square residuals and 1D velocity models

The first result of the survey was produced nearly in real time by Gudmundsson, who improved the automatic picks of the shots for the SIL stations and located the events using the SIL velocity model and only the sparse SIL setup (Fig. 6). The results demonstrate impressively the performance and restrictions of the permanent Icelandic network. While a near perfect reconstruction of the shot epicenter (<2 km lateral error) is available for the southernmost shots, a clear increase in error is observed for the shots along 67°N latitude and the shot close to Flatey Island, i.e. station FLA.

As stated above, about 1,000 events have been re-picked now including the whole temporary setup. They have been located with Hypoellipse (Klein 1984; Havskov and Ottemoller 2003). Only phase picks within 90 km distance from the epicenter were evaluated, because they do not include reflected or refracted phases from the Moho (see refraction seismics). Only picks with distances up to 30 km were weighted fully. No weighting was assigned to the picks according to individual pick quality. The epicenter was established and the depth was determined by a grid-search for minimum root-mean square travel time residual (from here abbreviated as RMS residual) This procedure was performed for four different velocity models (results see Fig. 5), the standard model for the SIL network based on Bjarnasson et al. (1993), a northern model from the SIL network (G. Gudmundsson, personal communication), the best fitting 1D LET model by Riedel et al. (2005) and a model derived from our refraction survey. All models (see Fig. 5) neglect the water layer above the ocean-bottom and surrounding the island stations.

Single errors for phases are commonly below 0.5 s, but about 10% of the S-phases for some OBS stations and SIL stations on the islands, FLA and GRI, cannot be decreased to an RMS residual below 0.8 s.

The average RMS residual value for the whole dataset is 0.274 (SIL), 0.255 (Northern SIL), 0.235 (LET) and 0.258 s (Refraction). Generally all models provide a good solution. The hypocenter distribution is very similar for the SIL and the Northern SIL model, but completely different for the LET model. Whereas events cluster in vertical bands between 5 and 15 km for the SIL models (Fig. 5), most events occur in a depth up to 3 km for the LET model (Fig. 7). However, just southeast of Grimsey a column of hypocenters increases the depth, above which 80% of the events are located (commonly interpreted as the brittle-ductile transition), to about 15 km just below the volcano-hydrothermal region (Fig. 7). Depths of the seismicity cut-off of about 10 km are also characteristic for the region north of Flatey.

Morphology and lithology

The overall morphology of the seafloor north of Iceland is well known, but it has never been available in such a resolution. Richter et al. (2003) already highlighted the pockmark structures, Brandsdottir et al. (2002) reported the bathymetric step associated with the HFF in Skjalfandi Bay. Cone structures in a pull-apart basin east of Grimsey were already noticed by Kuhn et al. (revised). The frequency and distribution of these cones has been described by Brandsdottir et al. (2002, 2004). Typical slope angles of ~30° and crater diameter to base diameter ratios fall well into the field for tuffcone like structures (Vespermann and Schmincke 2000). A number of surveys by Brands-

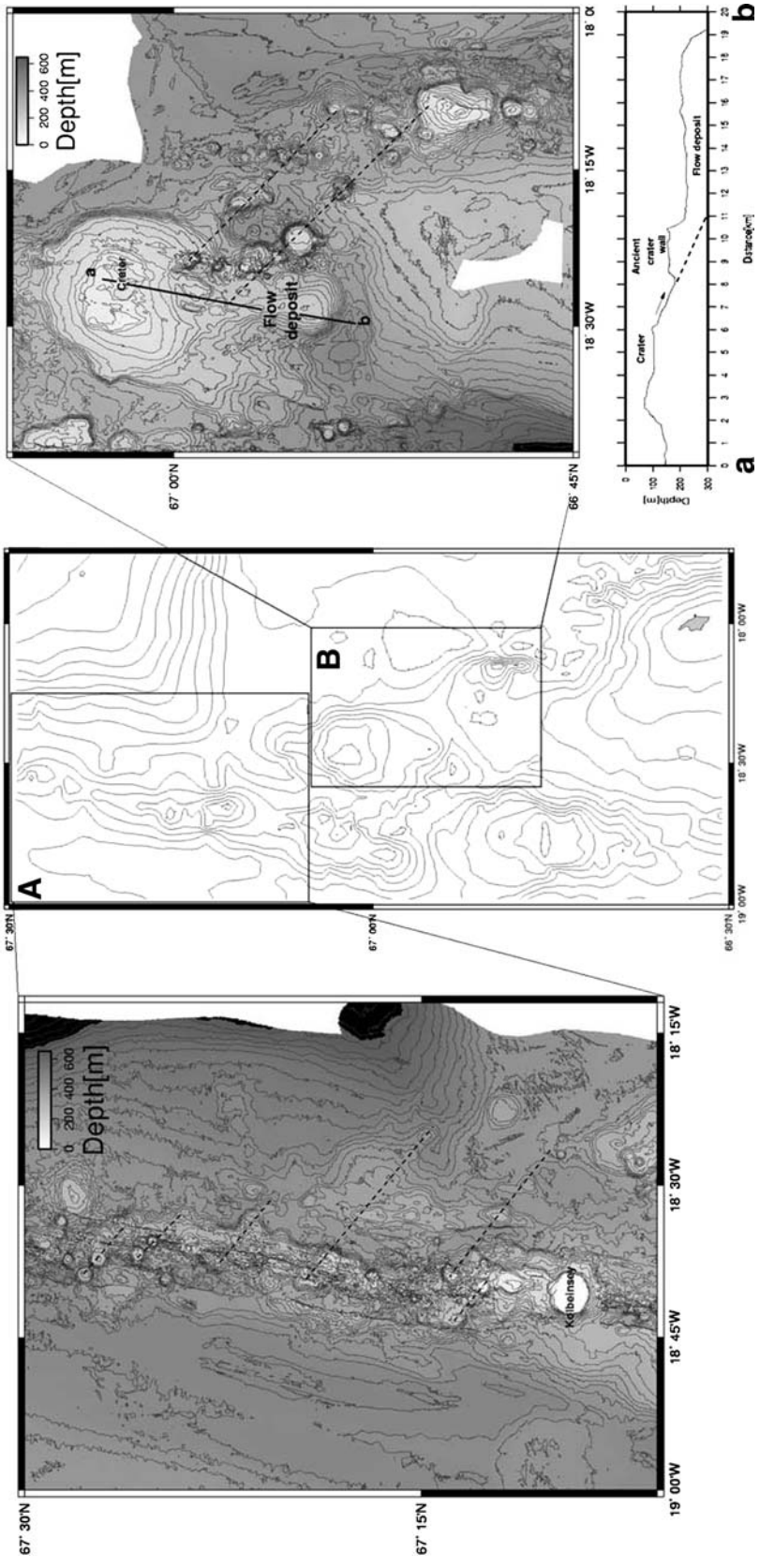

Fig. 8 Shows the interpolated multibeam bathymetry of (**A**) Kolbeinsey Ridge and (**B**) Storagrunn. The excerpts are marked on the central map. A profile and a preliminary interpretation for Storagrunn between points a and b is found at the *bottom right* of the figure

dottir et al. (2002, 2004) produced a multibeam beahymetric map of the region.

This survey filled the gap between Holl and Storagrunn volcanoes (Fig. 8b). A ridge of cones splits into two parallel rows of cones close to Storagrunn enclosing a small basin. Following the apex of the basin one can trace the center of the huge submarine volcano just NNW of it. Before the survey the top of Storagrunn was unknown and was suggested to consist of a crater valley. However, we were able to show that it is composed of a ragged top with only a small crater to the SSE, which is breeched to the SSW, probably by a huge flow deposit. The volcano flanks compose a horse-shoe of high flanks above a bathymetrically lower segment in the SSE toward the apex of the neighbouring basin.

Storagrunn was the main target for dredging. However, two dredge trials only revealed ice-rafted debris and/or beach gravel. During dredge along the eastern flank, which appeared to be formed recently, the dredge was lost in the sea.

A further focus of multibeam work was the Kolbeinsey ridge region between 19°W and 18°15′W south of 67°30′W. No ridge valley can be oberserved, but it was observed that the bathymetry becomes shallower toward the ridge. As well as the ridges of cones close to Storagrunn (dashed lines on Fig. 7b), cones on Kolbeinsey Ridge align with a strike of ~50°NW (dashed lines on Fig. 8a), which is subparallel to the more southerly GL (Fig. 8a).

Discussion

The newly acquired seismic data fit well to the past analysis of permanent SIL seismic data in the same region (Rögnvaldsson et al. 1998; Riedel et al. 2005), i.e. the 1D velocity model inverted by LET provides the smallest RMS residual. All tested velocity models allow a less erroneous locating process than the SIL model. The SIL model was optimized for South Iceland and our results indicate that the crustal structure from the north of Iceland differs from that in the south. However, it is obvious from Fig. 5, that the decisive factor for a discrimination of the models is the deep underground (>5 km), because above the models are very similar. Less erroneous locations favor a model with a velocity of 7 km/s or faster velocities from 10 km on.

The new locations cluster at lower depths, which also means that the brittle-ductile transition is more shallow than previously thought and the crust is thinner. These observations do not only fit the new velocity model, but also the old for South Iceland. So far, the high depths of earthquakes could not be explained easily. With the new data they disappear and do not need to be explained.

The velocity model from refraction also agrees well with these observations. South of the GL (Fig. 4b, dashed blue line in Fig. 5) no velocity higher than 7.3 km/s can be confirmed as a first arrival. The heterogeneity north and south of the lineament as depicted by deviations of the phase readings from the calculated arrival times using the best fit velocity models is very similar (Fig. 4). The region sampled in the south is much larger and some of the phases picked do not seem to be the first break. In contrast to the refraction model, the better LET 1D model was produced using events across the whole TFZ region, thus including information from both sides of the GL and is thus doomed to be better. Further more, the two models. LET and Refraction, are very similar up to a depth of 10 km (Fig. 5). The lower crust seems to indicate a subtle increase of velocity with depth, which prevents a first break from a Moho velocity around 8 km/s. In this case a LET will provide a much better model then refraction with our sparse shot dataset, so we do not want to discuss our models further.

We can also afford a glimpse further north. Our refraction model there (Fig.4a, solid blue line in Fig. 5) highlights a possible Moho in a bout 10 km depth with a velocity around 8 km/s, further north along the Southern Kolbeinsey Ridge the velocity model of the KRISE experiment (Hooft et al. 2006), reaches a velocity of 6.6–6.8 km/s at 3.5–4 km depth and the Moho at around 10–12 km depth which compares well with our 10 km. This might be evidence that there is a transition here from Icelandic crust underlain by an unknown, sometimes called transition, layer (Angenheister et al. 1980) to typical oceanic crust underlain by normal mantle material.

Our analysis shows that the SIL model still provides a good approximation for the epicenter in routine purposes. However, the depth of the sources differs strongly between the SIL and the best LET model. Most events seem to occur in a shallower subsurface than previously thought and only few events in the center of the research area occur deeper down (Fig. 7). This is in good agreement with the negative flower structure model (Woodcock and Fisher 1986) proposed by Riedel et al. (2001) based on fluid geochemistry. Having in mind, that the crust south of the HFF is not unusual for Icelandic crust and that the crust north of the GL is largely N-MORB, we conclude that the crust in between was and is still formed by a pull-apart process evoked by differential rifting of Kolbeinsey Ridge and the NVZ. The active pull-apart structures

are those where seismicity is most frequent and where fluids are migrating from the deep subsurface. The deepest active structures we could image are located along a line from Flatey to Grimsey in Skjalfandi trough.

Although we might only look at a snapshot in time of the seismicity, these results are supported by a LET based on data from the permanent network by Riedel et al. (2005), which show a low-velocity body in a depth of 7–12 km between Grimsey and Flatey, where the unusually deep seismicity is located. The presence of such a low-velocity body will actually mean that even the deep events found here are located in shallower positions.

The deepest reaching and most permeable and thus most probably most active fault of a flower structure is usually considered to be the principal rupture of the system (Barton et al. 1995). Here, this would refer to the GL, where the seimicity aligned at depth reaches its maximum. According to this hypothesis the rest of the seismicity is related to the near-surface Riedel shears at the edge of the pull-apart basin. Thus, the GL is rather a Grimsey Seismic Zone (GSZ) including a GL at its northeastern edge. In contrast to a classical flower structure as proposed by Woodcock and Fisher (1986), the main lineaments are not strike-slip faults with a dip-slip components, subparallel to the main rupture, but mainly dip-slip normal faults. Thus, our results clearly favor an extensional transform zone along the GSZ.

The high frequency of volcanic cones along the GL in contrast to the relatively flat surface along the HFF also suggests that volcanism and thus magmatic fluid migration mainly occurs within the GSZ. The alignment of cones further north on Kolbeinsey Ridge (Fig. 8), striking at a similar angle as the GL can only be produced by two scenarios.

- A strong influence of the transform shearing stress regime to the north, which produces strike-slip failure, or
- An asymmetric spreading where cones are transported obliquely away from the ridge center. This would imply that the Jan Mayen microplate to the east of Kolbeinsey Ridge is a growing plate, where more new crust is produced to the north of the plate to account for the oblique spreading.

In either case we find the influence of the transform regime still at a latitude of 67°30′N, far away from the Icelandic coastline. This implies that the crustal structure is changing smoothly toward the north and no sudden shift occurs at the GL.

Conclusions

We observe a transition from Kolbeinsey mid-ocean ridge crust to Icelandic crust along the GL, the northern limit of a GSZ. Whereas a mantle refraction could be identified for a region north of the GL, there is no confirmed mantle refractor south of it. The crust for this northern region is thinner than in Iceland and maybe even thinner than in the adjacent Kolbeinsey Ridge, though only slightly. South of the GL, there is a gradual increase in compressional wave velocity with depth starting at 4 km depth, implying that even at an offset of 140 km from the shot, there is no first break with a mantle velocity. A later arrival cannot be ruled out but could not be observed due to a low signal to noise ratio. In between the GL and the HFF, a main area of seismicity is located between Grimsey and Flatey Island running from north to south. Along this narrow line, the deepest hypocenters were recorded, whereas above it hypocenters spread out across the entire region in study, mostly clustering in north–south trending lineaments close to the surface. The Skjalfandi trough/basin complex resembles a classical negative flower structure as in the Woodcock and Fisher (1986) model. No petrological evidence for existing volcanism could be found from dredging, but multibeam bathymetry highlights some rough structures that appear to be recent. The opening of the flower structure produces a sharp contrast at the HFF with an origin in the stress regime of the GSZ, which can be traced up to 67°30′N and implies a gradual change in crustal structure toward Kolbeinsey Ridge.

Acknowledgments We thank Captains Ragnar G. D. Hermansson, and Gudmundur Bjarnasson and their crews for excellent support during the marine surveys. We ackowledge financial support by the Deutsche Forschungsgemeinschaft (DFG) under grants Da 478/13-1 and Ri 1220/2-1, the Swedish Vetenskapsradet, the Icelandic Research organization and the Leitstelle für mittelgrosse Forschungsschiffe for taking over the costs for the scientific cruises. Further more we are grateful for the access to instruments of the Geophysical Instrument Pool Potsdam, and for the shot permission and for the research permission to the Icelandic Research organization (RANNIS). C. Riedel also wants to thank Reinhard Wineberger at the german embassy in Reykjavik for unbureaucratic and fast support.

References

Angenheister G, et al. (1980) Reykjanes Ridge Iceland Seismic Experiment (RRISP 77). Z Geophys 47:228–238

Barton CA, Zoback MD, Moos D (1995) Fluid flow along potentially active faults in crystalline rock. Geology 23:683–686

Bjarnasson IT, Menke W, Flovenz OG, Caress D (1993) Tomographic image of the Mid-Atlantic plate boundary in southwestern Iceland. J Geophys Res 98:6607–6622

Björnsson A, Saemundsson K, Einarsson P, Tryggvason E, Grönvold K (1977) Current rifting episode in north Iceland. Nature 266:318–323

Botz R, Winckler G, Bayer R, Schmitt M, Schmidt M, Garbe-Schonberg D, Stoffers P, Kristjansson JK (1999) Origin of trace gases in submarine hydrothermal vents of the Kolbeinsey Ridge. Earth Planet Sci Lett 171:83–93

Brandsdottir B, Detrick R, Driscoll N, Kent G (2002) Pilot study of the Tjörnes fracture zone, offshore northern Iceland, using high-resolution multichannel seismic reflection profiling and CHIRP sonar. In: Proceedings of the AGU fall Meeting, San Francisco, 2001

Brandsdottír B, Richter B, Riedel C, Dahm T, Helgadottír G, Kjartansson E, Detrick R, Magnusson A, Ásgrimsson AL, Pálsson BH, Karson J, Saemundsson K, Mayer L, Calder B, Driscoll N (2004) Tectonic details of the Tjörnes Fracture Zone, an onshore-offshore ridge-transform in N-Iceland. Eos Trans AGU, 85(47):F1071

Caress DW, Chayes DN (1995) New software for processing sidescan data from sidescan-capable multibeam sonars. In: Proceedings of the IEEE Oceans 95 conference, San Diego, 997–1000

Cohen JK, Stockwell JW Jr (2003) CWP/SU: Seismic Unix release 37: a free package for seismic research and processing. Center for Wave Phenomena, Colorado School of Mines

Dahm T, Thorwart M, Flueh ER, Braun T, Herber R, Favali P, Beranzoli L, D'Anna G, Frugoni E, Smiriglio G (2002) Ocean bottom seismometers deployed in Turrhenian Sea. EOS Trans 83:309–314

Devey C, Garbe-Schonberg CD, Stoffers P, Chauvel C, Mertz DF (1994) Geochemical effects of dynamic melting beneath ridges: reconciling major and trace element variations in Kolbeinsey (and global) mid-ocean ridge basalts. J Geophys Res 99(B5):9077–9095

Earle PS, Shearer PM (1994) Characterization of global seismograms using an automatic picking algorithm. Bull Seismol Soc Am 84(2):366–376

Gudmundsson A, Brynjolfsson S, Jonsson MT (1993) Structural analysis of a transform fault-rift zone junction in North Iceland. Tectonophysics 220:205–221

Geirsson H (2002) Continuous GPS measurements in Iceland 1999–2002. MSc thesis, University of Iceland

Havskov J, Ottemoller L (2003) SEISAN: the earthquake analysis software, Version 8.0 preliminary, University of Bergen, http://www.ifjf.uib.no/Seismologi/software/seisan/seisan.html

Hooft E, Brandsdottir B, Mjelde R, Shimamura H, Murai Y (2006) Asymmetric plume-ridge interaction around Iceland: the Kolbeinsey Ridge Iceland Seismic Experiment. Geochem Geophys Geosyst 7:Q05015; doi:10.1029/2005GC001123

Hole J, Beaudoin BC, Klemperer SL (2000) Vertical extent of the newborn San Andreas fault at the mendocino triple junction. Geology 28:1111–1114

Klein FW (1984) User's guide to HYPOINVERSE, a program for VAX and PC 350 computers to solve for earthquake locations, USGS open file report-84-000

Kuhn T, Riedel C, Herzig PM, Theilen F (revised) Shallow 3d structure of the Grimsey Lineament offshore North Iceland. Mar Geol

McMaster RL, Schilling J-GE, Pinet PR (1977) Plate boundary within Tjörnes fracture zone on northern Iceland's insular margin. Nature 269:663–668

Richter B, Driscoll N, Detrick R, Fornari D, Brandsdottir B (2003) Recently discovered near-shore gas-charged sediments and pockmarks, northern Iceland. In: Proceedings of the AGU fall. Cite abstracts as: Eos Trans AGU, 84(46), Fall Meet Suppl Abstract AGUFMOS51B0854R

Riedel C, Schmidt M, Botz R, Theilen F (2001) The grimsey hydrothermal field offshore North Iceland: crustal structure, faulting and related gas venting. Earth Planet Sci Lett 193:409–421

Riedel C, Tryggvason A, Dahm T, Stefansson R, Bödvarsson R, Gudmundsson GB (2005) The seismic velocity structure north of Iceland. J Seismol 5:383–404

Rögnvaldsson ST, Gudmundsson A, Slunga R (1998) Seismotectonic analyses of the Tjörnes fracture zone, an active transform fault in north Iceland. J Geophys Res 103:30117–30129

Sæmundsson K (1974) Evolution of the axial rifting zone in northern Iceland and the Tjörnes fracture zone. GSA Bull 85:495–504

Stoffers P, Botz R, Garbe-Schonberg G, Hannington M, Hauzel B, Herzig P, Hissmann K, Huber R, Kristjansson JK, Petursdottir SK, Schauer J, Schmitt M, Zimmerer M (1997) R/V Poseidon, Cruise report 229a. Institut fur Meereskunde, Universitaet Kiel

Taylor B, Crook K, Sinton J (1994) Extensional transform zones and oblique spreading centers. J Geophys Res 99(B10):19707–19718

Thoroddsen T (1925) Die Geschichte der islandischen Vulkane, K. Dan. Vidensk. Skr., 9. Raekke, Naturvidensk. Mat. Afd., 8, Copenhagen

Thorwart M, Dahm T (2003) Evaluation of ringing-phases on ocean-bottom seismometer, EGS-AGU-EUG joint assembly. Nice, France, 6–11 April 2003

Vespermann D, Schmincke H-U (2000) Scoria cones and tuff rings. In: Sigurdsson H, Houghton B, McNutt S, Rymer H, Stix J (eds) Encyclopedia opf volcanoes. Academic Press, New York, pp683–694

Vogt P, Johnson GL, Kristjansson L (1980) Morphology and magnetic anomalies north of Iceland. J Geophys 47:767–780

Woodcock NH, Fisher M (1986) Strike-slip duplexes. J Struct Geol 8:725–735